Bioorganic Chemistry 105 (2020) 104373

Contents lists available at ScienceDirect

Bioorganic Chemistry

journal homepage: www.elsevier.com/locate/bioorg

Potent human dihydroorotate dehydrogenase inhibitory activity of new quinoline-4-carboxylic acids derived from phenolic aldehydes: Synthesis, cytotoxicity, lipophilicity and molecular docking studies

Milena M. Petrović [a], Cornelia Roschger [b], Sidrah Chaudary [b], Andreas Zierer [b], Milan Mladenović [a], Katarina Jakovljević [a], Violeta Marković [a], Bruno Botta [c], Milan D. Joksović [a,*]

[a] Faculty of Sciences, Department of Chemistry, University of Kragujevac, R. Domanovica 12, 34000 Kragujevac, Serbia
[b] University Clinic for Cardiac-, Vascular- and Thoracic Surgery, Medical Faculty, Johannes Kepler University Linz, Krankenhausstraße 7a, 4020 Linz, Austria
[c] Dipartimento di Chimica e Tecnologie del Farmaco, Sapienza Università di Roma, P.le Aldo Moro 5, 00185 Roma, Italy

ARTICLE INFO

Keywords:
Dihydroorotate dehydrogenase (DHODH)
hDHODH inhibitors
Quinoline-4-carboxylic acid
Cytotoxicity
Lipophilicity
Molecular docking

ABSTRACT

A series of novel 2-substituted quinoline-4-carboxylic acids was synthesized by Doebner reaction starting from freely available protocatechuic aldehyde and vanillin precursors. Human dihydroorotate dehydrogenase (hDHODH) was recognised as a clear molecular target for these heterocycles. All compounds were also tested for their antiproliferative potential against three cancer cells (MCF-7, A549, A375) and one normal cell line (HaCaT) to evaluate the selective cytotoxicity. Quinoline derivatives **3f** and **3g** were identified as potent hDHODH inhibitors while **3k** and **3l** demonstrated high cytotoxic activity against MCF-7 and A375 cells and good selectivity. In addition, the $logD_{7.4}$ values obtained by the experimental method were found to be in the range from −1.15 to 1.69. The chemical structures of all compounds were confirmed by IR, NMR and elemental analysis. The compounds pharmacology on the molecular level was revealed by means of molecular docking, highlighting the structural differences that distinguish highly active from medium and low active hDHODH inhibitors.

1. Introduction

Human dihydroorotate dehydrogenase (hDHODH), as one of the most important enzymes in sustaining the proliferation of cancer cells, represents a good target for chemotherapeutic drugs [1]. In the fourth step of the *de novo* biosynthesis of pyrimidines, this redox enzyme catalyses the oxidation of dihydroorotate to orotate mediated by flavin mononucleotide and nicotinamide adenine dinucleotide or ubiquinone. This essential conversion allows cells to synthesize uridine monophosphate, a vital building block in the formation of ribonucleosides and deoxyribonucleosides for RNA and DNA synthesis [2,3]. In the proliferation stage, the cells depend on *de novo* nucleoside biosynthesis and as a result, DHODH is frequently overexpressed in cancer cells to support their growth. Moreover, DHODH is not only considered as a key enzyme in the treatment of cancer, but also a potential target for malaria [4], viral [5] and autoimmune diseases, such as rheumatoid arthritis or multiple sclerosis [6].

The essential role of pyrimidine nucleotides for cell proliferation and multiplication determines hDHODH as the main target for design and synthesis of new drug candidates. In an increased demand for DNA, RNA, glycoproteins and membrane lipids, proliferating cells depend heavily on pyrimidine biosynthesis pathway [7]. Inhibition of hDHODH causes an insufficient concentration of pyrimidine nucleotides required for continued growth and in turn triggers various cytotoxic, antimalarial, antifungal and immunosuppressive activities [8,9].

Various hDHODH inhibitors have been synthesized, out of which brequinar, leflunomide and its active metabolite teriflunomide have gained a lot of interest over the several past decades (Fig. 1). Leflunomide, an isoxazole-based prodrug, is FDA approved for rheumatoid and psoriatic arthritis, while teriflunomide is FDA approved for multiple sclerosis [10]. Brequinar is a fluorinated quinoline-4-carboxylic acid derivative with potent antineoplastic activity in numerous *in vitro* experiments and cancer models. Despite of the impressive preclinical evaluation, brequinar did not meet objective response in multiple phase

* Corresponding author.
E-mail address: mjoksovic@kg.ac.rs (M.D. Joksović).

https://doi.org/10.1016/j.bioorg.2020.104373
Received 10 March 2020; Received in revised form 25 September 2020; Accepted 8 October 2020
Available online 12 October 2020

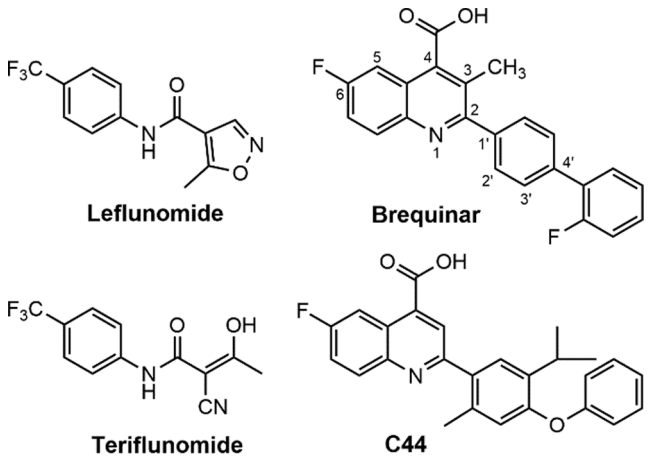

Fig. 1. Chemical structures of the selected hDHODH inhibitors.

II clinical trials for several types of solid tumors [1]. However, the recent studies demonstrated better suitability of brequinar for non-solid tumors, particularly in induced differentiation of AML cells both *in vivo* and *in vitro* assays [11,12]. Also, synergistic action of brequinar with oxaliplatin and gemcitabine was observed *in vitro* in KRAS mutant cells [13]. Therefore, these studies highlight promising perspectives for brequinar and other hDHODH inhibitors containing quinoline-4-carboxylate scaffold. The quinoline-4-carboxylic acid derivative C44 is one of the most potent compounds that inhibits hDHODH with IC_{50} of 1 nM [14]. This hindered ether fragment with the restricted rotation across the diaryl ether bond having required hydrophobicity, is crucial for an excellent enzyme inhibition.

Bearing in mind these facts, we envisioned that two neighbouring alkyl/aryl ether units combined with quinoline scaffold may also result in good DHODH activity and favourable pharmacological profile. Consequently, we have prepared a series of novel 2-substituted quinoline-4-carboxylic acids involving two alkyl/aryl ether linkages. The simple alkylation of freely available phenolic aldehydes and then a three-component Doebner reaction of previously alkylated aldehydes, aniline and pyruvic acid afforded the desired compounds with potent hDHODH activity. The results also reported antiproliferative potential against three cancer cell lines and selective cytotoxicity. To validate DHODH as the target of our compounds, here we report a pictorial presentation of the docked poses for the most active compounds.

2. Results and discussion

2.1. Chemistry

Pfizinger and Doebner reactions are two possible ways to introduce a carboxylic acid function in the 4-position of quinoline scaffold. The former is based on the condensation of isatin with a carbonyl compound in the presence of suitable strong base [15]. However, this synthetic route suffers from a long reaction time, the poor availability of isatin and low reaction yields. Several quinoline-4-carboxylic acid derivatives with excellent DHODH inhibitory activity were prepared in this manner in 10–47% yields and 12–48 h of reflux [14,16]. The Doebner reaction is another method of forming 2-substituted quinoline-4-carboxylic acids starting from anilines, benzaldehydes and pyruvic acid [17]. Unfortunately, low yields, particularly for di- or trisubstituted aldehydes, and expensive catalysts [18] have also limited this route for the synthesis of the various quinoline heterocycles. Thus, the selection of readily available and relatively cheap starting carbonyl and amine precursors could increase an attractability and usability of Doebner reaction.

The first step in our synthesis of 2-substituted quinoline-4-carboxylic acids was based on alkylation of commercially available vanillin and protocatechuic aldehyde by different alkyl halides according to the known procedure [19]. The reaction was performed in *N*,*N*-dimethylformamide as a solvent and $NaHCO_3$ was used to neutralize liberated HCl. In the next step, Doebner multicomponent reaction was applied to prepare target compounds. Aniline, pyruvic acid and various *O*-alkylated aldehydes were refluxed in ethanol for 3 h affording the final quinoline-4-carboxylic acids in yields from 24% to 51% (Scheme 1). All compounds easily crystalized from ethanolic solution, sometimes after scratching the bottom or side of the flask whit a glass rod, and were satisfactory pure. The very high purity was achieved by their dissolving in chloroform and precipitation by hexane or by recrystallization from ethanol. The chemical structures of all quinoline derivatives were confirmed by elemental analysis, IR, ^1H and ^{13}C NMR data (Supporting Information).

2.2. Biological studies

2.2.1. Inhibition of hDHODH

The inhibition of human dihydroorotate dehydrogenase (hDHODH) activity by the compounds was determined using the DHODH biochemical assay. This is an indirect colorimetric method which is based on the oxidation of L-dihydroorotic acid (L-DHO) aided by reduction of decylubiquinone (DUQ) which is stoichiometrically equivalent to reduction of 2,6-dichloroindophenol (DCIP) resulting in the decrease in absorbance at 610 nm [7]. The results of enzyme inhibitory activity are presented in Table 1. Most quinoline-4-carboxylic acids exhibited lower IC_{50} values than drug leflunomide used as a reference compound. Quinoline derivatives from protocatechuic aldehyde series (**3d**, **3e**, **3f** and **3g**) showed better activity than compounds synthesized from alkylated vanillin (**3h**, **3i**, **3j**, **3k** and **3l**).

The tested compounds were not so potent as brequinar, a well known hDHODH inhibitor with an IC_{50} of 5–10 nM [20]. As expected, a replacement of the conformationally flexible alkoxy groups in our series with the planar phenyl substituent in brequinar allows stacking interactions resulting in a significant potency. Activity differences between brequinar containing the terminal 2-fluorophenyl substituent and 3′,4′-disubstitution may be attributed to effects that lower the total number of conformations of the terminal phenyl ring. The similar observations were reported for quinoline-4-carboxylates bearing terminal 2-substituted pyridine ring [16]. In addition, the fluorine at 6-position of quinoline scaffold in brequinar molecule has also a contribution to its high hDHODH activity.

2.2.2. Cytotoxicity

Cytotoxicity of the compounds against the human breast adenocarcinoma cell line MCF-7, human lung adenocarcinoma cell line A549, human melanoma cell line A375 and the non-cancerous human keratinocyte cell line HaCaT was evaluated using the 3-(4,5-dimethylthiazol-2-yl)-2,5-diphenyltetrazolium bromide (MTT) assay. The results of antiproliferative activity *in vitro* are expressed as IC_{50}, the concentration of compound (μM) that inhibits survival of the cells by 50% as compared to control untreated cells (Table 2). MCF-7 and A375 cancer cells were the most sensitive to the antiproliferative action of quinoline-4-carboxylic acids.

The selectivity index (SI) is the ratio of the IC_{50} values for the MCF-7, A549 and A375 cancer cell lines to the IC_{50} value for the normal HaCaT cells (Table 3).

The greater value of SI indicates less toxic compound to the normal cells offering a safer potential therapy. The compounds with SI higher than 10 could be considered as selective ones. The quinoline derivative **3k** from vanillin series displayed the highest SI ranging from 22.0 (A375 cells) to 26.0 (MCF-7 cells). The SI value from 0.82 to 4.64 suggests that the compounds **3a-n** cannot successfully differentiate between normal and A549 cancer cell lines.

2.2.3. SAR studies

Three principal regions in the molecule of quinoline-4-carboxylic

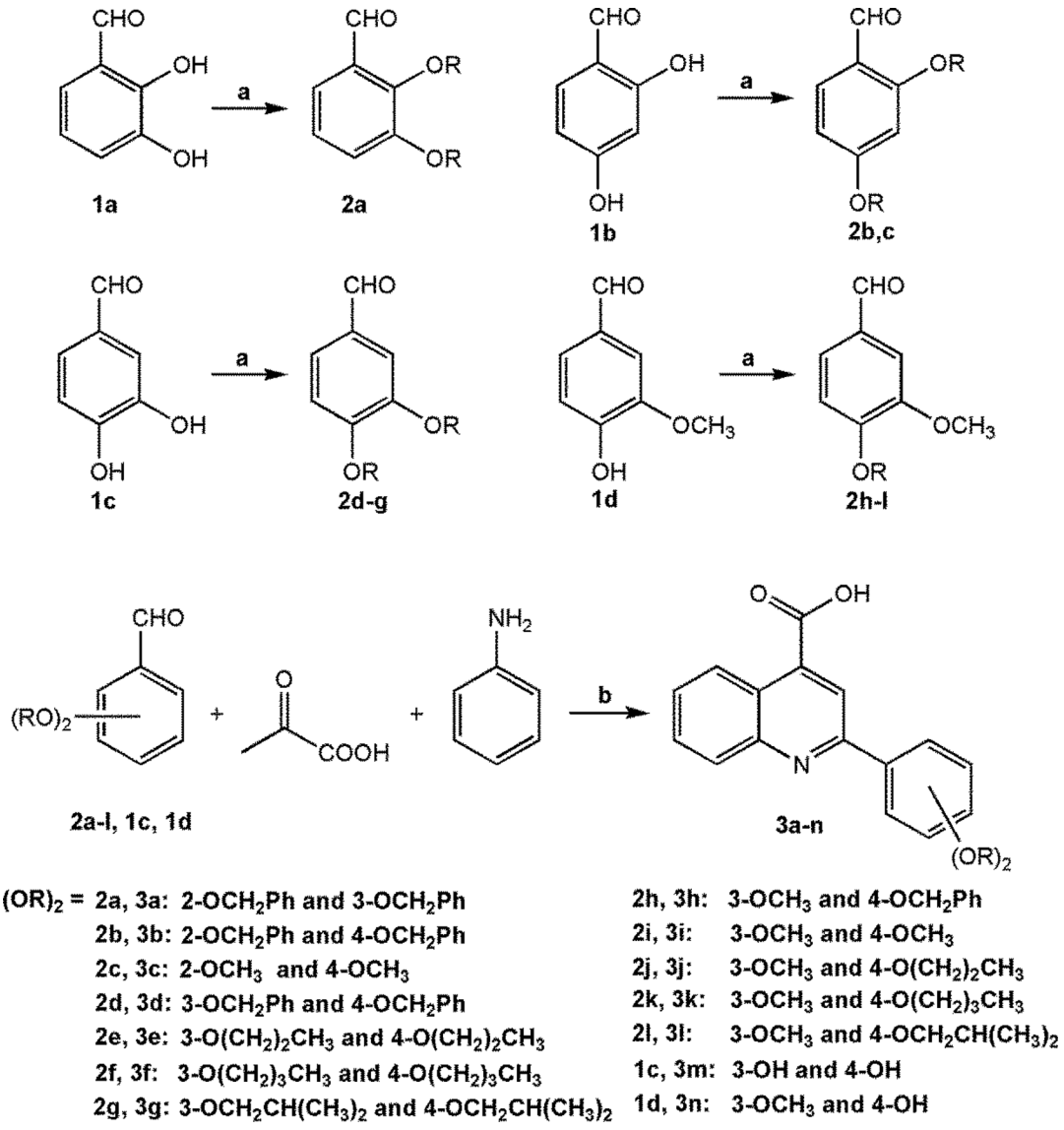

Scheme 1. Reagents and conditions: a) alkyl halide (MeI, ^{n}PrBr, ^{n}BuBr, ^{i}BuBr or BnCl), K_2CO_3, DMF, 5 h, reflux, HCl; b) EtOH, 3 h, reflux.

Table 1
Inhibition of human dihydroorotate dehydrogenase (hDHODH) by quinoline-4-carboxylic acid derivatives **3a-n**.

Compd.	IC_{50} ± SD (μM)	Compd.	IC_{50} ± SD (μM)
3a	0.268 ± 0.018	**3i**	1.387 ± 0.733
3b	0.340 ± 0.027	**3j**	0.449 ± 0.039
3c	2.549 ± 0.193	**3k**	0.340 ± 0.033
3d	0.270 ± 0.021	**3l**	0.438 ± 0.033
3e	0.384 ± 0.029	**3m**	1.073 ± 0.105
3f	0.153 ± 0.009	**3n**	0.944 ± 0.047
3g	0.148 ± 0.009	**leflunomide**	0.900 ± 0.068
3h	0.467 ± 0.036	**brequinar**	0.010 ± 0.005

Table 2
IC_{50} values (μM) found for the MCF-7, A549, A375 and normal HaCaT cell lines after treatment with the quinoline-4-carboxylic acids **3a-n**.

Compd.	IC_{50} ± SD (μM)			
	MCF-7	A549	A375	HaCaT
3a	3.44 ± 0.80	19.88 ± 0.02	5.67 ± 2.07	21.19 ± 8.32
3b	3.21 ± 1.08	19.36 ± 0.03	4.67 ± 1.55	15.80 ± 6.51
3c	19.54 ± 8.90	30.11 ± 0.03	34.08 ± 11.82	54.49 ± 13.87
3d	3.29 ± 0.75	12.49 ± 0.07	3.50 ± 0.73	20.08 ± 9.97
3e	6.78 ± 2.15	13.26 ± 0.04	7.91 ± 3.31	30.90 ± 9.34
3f	3.47 ± 0.91	10.75 ± 0.07	5.42 ± 1.14	22.62 ± 7.76
3g	2.52 ± 0.72	13.79 ± 0.05	1.52 ± 0.44	11.93 ± 5.47
3h	6.61 ± 2.79	24.86 ± 0.05	6.79 ± 2.70	69.50 ± 15.45
3i	12.56 ± 5.86	37.90 ± 0.06	23.23 ± 7.08	41.62 ± 11.42
3j	7.28 ± 2.91	15.07 ± 0.05	2.69 ± 0.58	36.13 ± 10.63
3k	4.14 ± 1.72	24.03 ± 0.02	4.88 ± 1.81	107.50 ± 20.49
3l	1.77 ± 0.57	8.96 ± 0.05	3.48 ± 1.38	32.85 ± 13.97
3m	12.21 ± 5.20	9.37 ± 0.05	14.74 ± 6.36	43.44 ± 11.37
3n	10.06 ± 4.70	22.71 ± 0.02	6.15 ± 2.34	57.48 ± 13.06

acid derivatives are responsible for enzyme activity: (i) there is a strict requirement for carboxylic acid at the C-4 position (see the atom numbering of the brequinar molecule in Fig. 1); (ii) a phenyl group at the C-2 position with hydrophobic substituents is necessary and (iii) fluorine or strong electron-withdrawing trifluoromethyl group at the C-6 position have a beneficial effect for inhibitory activity [21]. Although fluorine is widely used in drug synthesis to improve activity, the novel investigation highlights "the dark side of fluorine" [22]. Drug-metabolizing enzymes can promote oxidative defluorination and release fluoride generating various toxic effects. Very often, fluorine-containing chemotherapeutics are usually highly toxic against normal cell lines and exhibit low selective cytotoxicity [23]. For these reasons,

Table 3
Selectivity of the cytotoxicity of the compounds 3a-**n** against tumor cells as compared with HaCaT cells.

Compd.	Selectivity index (SI)		
	MCF-7	A549	A375
3a	6.16	1.07	3.74
3b	4.92	0.82	3.38
3c	2.79	1.81	1.60
3d	6.10	1.61	5.74
3e	4.56	2.33	3.91
3f	6.52	2.10	4.17
3g	4.73	0.87	7.85
3h	10.51	2.80	10.24
3i	3.31	1.10	1.79
3j	4.96	2.40	13.43
3k	25.97	4.47	22.03
3l	18.56	3.67	9.44
3m	3.56	4.64	2.95
3n	5.71	2.53	9.35

we designed the synthesis of quinoline-4-carboxylic acids omitting fluorine at the C-6 position in order to achieve better selective cytotoxicity and minimize toxic side effects.

Our initial intention was to validate how the different position of two benzyloxy groups in the compounds **3a**, **3b** and **3d** influences on cytotoxic and DHODH inhibitory activity (Table 1). The analogue **3d** was the most active against A549 and A375 cell lines with the best selectivity index (SI) and consequently its protocatechuic and vanillin precursors (**1c** and **1d**) were selected for further derivatization. Interestingly, **3a** (2′,3′-disubstitution) and **3d** (3′,4′-disubstitution) displayed the same DHODH activity with an IC_{50} = 0.27 μM. When benzyloxy group was replaced by methoxy substituent (**3c**), a substantial loss of cytotoxic and enzyme inhibitory activity was observed. Further syntheses were performed to see the effects of a series of 3′,4′-disubstituted quinoline compounds for antiproliferative potential and enzyme inhibition. The synthesized analogues **3f** and **3g** containing *n*-butyl and isobutyl groups at C-3′ and C-4′ position respectively, were the most potent in DHODH assays with IC_{50} = 0.15 μM. The derivatives **3f** (IC_{50} = 3.47 μM against MCF-7 and IC_{50} = 5.42 μM against A375 cells) and **3g** (IC_{50} = 2.52 μM against MCF-7 and IC_{50} = 1.52 μM against A375 cells) were found to show strong antiproliferative potential. Unfortunately, the selectivity index for these two compounds was relatively low; the **3g** with bulkier hydrophobic isobutyl group was two-fold more toxic against normal HaCaT cells than **3f** with *n*-butyl one. A comparison between **3f** and **3g** suggests that substituent size and steric effects may be a contributing factor to degrees of conformational freedom in antiproliferative action of these compounds. The quinoline compound **3k**, prepared from *n*-butylated vanillin precursor resulted in the lowest cytotoxicity against normal HaCaT cells (IC_{50} = 107.50 μM), good antiproliferative activity against MCF-7 and A375 cells with IC_{50} = 4.14 μM and IC_{50} = 4.88 μM, respectively and excellent DHODH inhibition (IC_{50} = 0.340 μM). The quinoline-4-carboxylic acids **3m** and **3n** synthesized from non-alkylated phenolic aldehyde precursors demonstrated a significant decrease in the antiproliferative and DHODH inhibitory potency. The compound **3l** prepared from isobutylated vanillin demonstrated lower DHODH activity (IC_{50} = 0.44 μM) compared to **3g** synthesized from isobutylated protocatechuic aldehyde (IC_{50} = 0.15 μM). However, **3l** was also very effective against MCF-7 (IC_{50} = 1.77 μM) and A375 cancer cells (IC_{50} = 3.48 μM) with significant selectivity index (18.6 and 9.4 respectively). The presence of two hydrophobic groups at the 3′ and 4′ position (**3g**) led to increased cytotoxicity against the normal HaCaT cells in comparison with compound **3l** containing only one hydrophobic substituent. Generally, all compounds from vanillin series except **3i** (**3h**, **3j**, **3k** and **3l**) showed better selectivity than **3d**, **3e**, **3f** and **3g** from protocatechuic aldehyde series indicating more favourable pharmacological profile for quinolines derived from vanillin. Unfortunately, there is no available cytotoxic data of other quinoline-4-carboxylic acids against normal cells for further comparison with our compounds. The compound **3i** with two methoxy groups at the 3′ and 4′ position displayed moderate DHODH inhibition and low selectivity index. The polar hydroxyl groups in **3m** and **3n** were not able to allow the required strong hydrophobic interaction between these two compounds and enzyme. Evidently, cytotoxic and enzyme inhibition data suggest that the presence of at least one hydrophobic group at the C-3′ and C-4′ position is necessary to retain the good biological activity.

Analysing the results from Tables 1 and 2, we can postulate that better DHODH inhibition leads to better cytotoxic activity. These data indicate that DHODH inhibition correlates with decreased tumor cell growth, especially in MCF-7 and A375 cell lines.

2.2.4. *Lipophilicity study*

In the drug discovery process, the optimization of solubility and lipophilicity plays an important role due to the close association of these properties with the absorption, distribution, metabolism, excretion, and toxicity (ADMET) of compounds [24]. High target potency in combination with high lipophilicity may increase the risk of ADMET-related damage by enhancing drug promiscuity and nonspecific toxicity [25]. Therefore, balanced optimization is of great importance in the synthesis of compounds with good pharmacological profile. The main goal of optimization is to achieve good potency without significantly increasing lipophilicity at the same time.

One of the most important stages in the drug discovery process is based on the drug absorption through membrane via passive diffusion. In order to facilitate absorption, drugs should be lipophilic enough to penetrate the lipid cores of membranes, but not too lipophilic that they remain there. Therefore, lipophilicity as the measure of drug affinity for a lipid environment plays a crucial role in the pharmaceutical industry because it indicates the relationship of drugs with their pharmacokinetic and metabolic properties [26]. Lipophilicity can be measured by the distribution of a compound between the nonpolar organic phase (*n*-octanol) and the aqueous phase. The partition coefficient P represents the ratio of the equilibrium concentrations of a dissolved compound in each phase and can be determined by a variety of methods [27]. However, when an ionisable compound is equilibrated in this two-phase system, its concentration is directly related to the distribution coefficient D which is the partition coefficient of the compound in both neutral and ionized form at any pH. The logD at pH = 7.4 has the highest importance because of its physiological relevance and resemblance to real biological partitions.

Highly lipophilic compounds ($logD_{7.4}$ > 3.5) tend to have poor aqueous solubility, high binding to plasma proteins, and greater potential to inhibit Cytochrome P450 enzymes and interactions with P-glycoproteins increasing the risk of drug-drug interactions. The moderate lipophilicity ($logD_{7.4}$ = 0–3) represents an excellent balance between permeability and solubility having low metabolic liability. These $logD_{7.4}$ values are favourable for BBB (blood-brain barrier) penetration allowing an optimal oral absorption and cell membrane permeation in cell-based assays. The negative values of logD in the physiologically relevant pH lead to higher aqueous solubility and poor permeability through biological membranes limiting the transport across the blood-brain barrier [28].

Since all our synthesized quinoline-4-carboxylic acids **3a-n** are at least partly charged at physiological pH (7.4) due to presence of ionisable carboxylic group, logD is the accurate descriptor of compound lipophilicity as it describes the partition of both unionized and ionized forms. Consequently, we measured the lipophilicity of our compounds by their distribution between phosphate buffer at 7.4 (aqueous phase) and *n*-octanol as an immiscible organic solvent. In the typical shake-flask method, after vigorous mixing and phase separation, the compound concentration in both solvents was measured by UV–Vis spectrophotometry and $logD_{7.4}$ was calculated using the equation $logD_{7.4} = logC_{oct}/C_{buffer}$.

Among all enzymes of *de novo* biosynthesis of pyrimidines, only

DHODH is located on the outer surface of the inner mitochondrial membrane and drugs must be able to reach to mitochondria to inhibit this enzyme. Thus, the lipophilic properties of the potential inhibitors will strongly influence on DHODH activity. The results presented in Table 4 show that the least lipophilic compounds were those containing polar hydroxyl and/or methoxy substituents (**3c**, **3i**, **3m** and **3n**), showing negative $logD_{7.4}$ values from −1.15 to −0.37. As it was expected, the incorporation of more hydrophobic groups into the molecular structure enhanced the lipophilicity, but also caused an increase in the DHODH inhibitory activity. The derivatives **3f** and **3g** containing *n*-butyl and isobutyl groups displayed the best DHODH activity with $logD_{7.4} = 1.49$ and 1.44, respectively. We observed this range of $logD_{7.4}$ values as optimal for an excellent DHODH inhibition. The higher value of $logD_{7.4}$ (**3e**, $logD_{7.4} = 1.69$) and lower one (**3d**, $logD_{7.4} = 1.34$) led to decrease of DHODH inhibitory activity. It is interesting to note that **3e** with two *n*-propyl groups at 3′ and 4′ position ($logD_{7.4} = 1.69$) was more lipophilic than **3f** and **3g** with *n*-butyl and isobutyl substituents. This behaviour can be explained by conformational reasons where the most abundant conformers in *n*-octanol have slightly lower hydrophobicity due to interaction of vicinal alkyl chains in **3f** and **3g** [29]. The compounds from vanillin series except **3i** (**3h**, **3j**, **3k**, and **3l**) had lower lipophilicity with $logD_{7.4}$ from 0.33 to 1.06, still retaining good IC_{50} values for enzyme inhibition from 0.34 μM to 0.47 μM. Evidently, the lipophilicity strongly affected DHODH inhibition and this dependence for 3′,4′-disubstituted derivatives of 2-phenylquinoline-4-carboxylic acids is presented graphically in Fig. 2 with relatively good correlation coefficient $r = 0.76$.

Experimentally determined antiproliferative activity of our compounds showed certain dependence on lipophilicity versus IC_{50} values, although a linear correlation was very weak (A549 cells) to moderate (MCF-7 cells) with coefficient $r < 0.55$. Except **3h**, *in vitro* cytotoxic activity is significantly controlled by lipophilicity in the range of $logD_{7.4}$ from 0.95 to 1.49 (**3a**, **3b**, **3d**, **3f**, **3g** and **3l**). This indicates that an easier transport over membrane barriers at cellular level can eventually lead to cell death. The most lipophilic compound **3e** with $logD_{7.4} = 1.69$ demonstrated lower activity against all types of cell lines. On the other side, **3m** with negative logD value (−1.15) had very similar cytotoxic activity against A549 cells compared to **3l** with $logD_{7.4} = 0.95$. It means that lipophilicity is important, but only one of factors influencing the cytotoxic activity.

2.2.5. Molecular docking studies

Having determined that structurally optimized quinoline-4-carboxylic acids were notable hDHODH inhibitors, their pharmacology was further considered on the structure-based level. In that sense, to perform a quality structure-based activity relationship analysis, a profound knowledge of hDHODH tertiary structure is required. Thus, the resolved X-ray hDHODH topography [30] accentuates two domains: a small *N*-terminal domain compiled of residues Met30-Leu68, and a larger *C*-terminal domain formed of residues Met78-Arg396, interconnected by an extended loop. The C-terminal domain is an α helices/β strands conglomerate with a central barrel of eight parallel β strands surrounded by eight α helices. Within the tertiary topography, two are the sites responsible for biochemical role of hDHODH: (1) a redox site, made of three antiparallel strands (βC, βD and βE) at the top and two antiparallel strands (βA and βE) at the bottom, that serves as nesting area for the dihydroorotate as substrate and flavin mononucleotide (FMN) binding site as cofactor; (2) a narrow tunnel within the *N*-terminus, through which the ubiquinone easily approaches the FMN for the redox reaction. From the crystallography point of view, the narrow tunnel is the very target for inhibiting the hDHODH activity [30]. By accepting the ubiquinone as the second cofactor, the *N*-terminal domain fulfils its biochemical purpose: by virtue of two joined constitutive α helices (labelled α1 and α2) it is a connector between the enzyme and the internal mitochondrial membrane. In other words, being immersed into the mitochondrial membrane, distinct helices form a tunnel that harbours the FMN binding site and accepts the ubiquinone. Thus, further rationalization of the *N*-terminal domain topography provides a basis for understanding the mode of action of potential hDHODH inhibitors. The tunnel's sub-site 1 is almost exclusively complied of hydrophobic residues Leu42, Met43, Leu46, Gln47, Ala55, Leu58, Phe62, Leu68, Phe98, and Leu359, which are, as α1 and α2 helices foundations, involved in membrane association. In between the tunnel and the afore mentioned redox site there are sub-sites 2 and 3, formed of Gln47, Arg136, Tyr356 and Thr360. The amino acids Val134 and Val143 create hydrophobic sub-site 4 that caps the narrow end of the tunnel.

The entire molecular docking-based discussion is performed by respecting the decreasing order of hDHODH inhibitors activity. All of the best-clustered conformations were comparable with the previously experimentally determined crystals structures of either clinical drug leflunomide (PDB ID **3F1Q**) [30] or co-crystalized 4-quinoline carboxylic acid derivatives, brequinar (PDB ID **1D3G**) [31], **43** and **46** (PDB IDs **6CJF** and **6CJG**, respectively) [16]. Hence, being reversibly associated to the hDHODH, the herein most active hDHODH inhibitor **3g** (Fig. 3) occupies almost entirely the narrow tunnel. Thus, compound adopts a biopose in which the C-4 carboxylic acid forms a strong hydrogen bond ($d_{HB} = 2.648$ Å) with one of the Arg136′s guanidino ω-nitrogens (ω-*N*), *via* the carbonyl moiety. The same ω-*N* is a hydrogen bond donor for

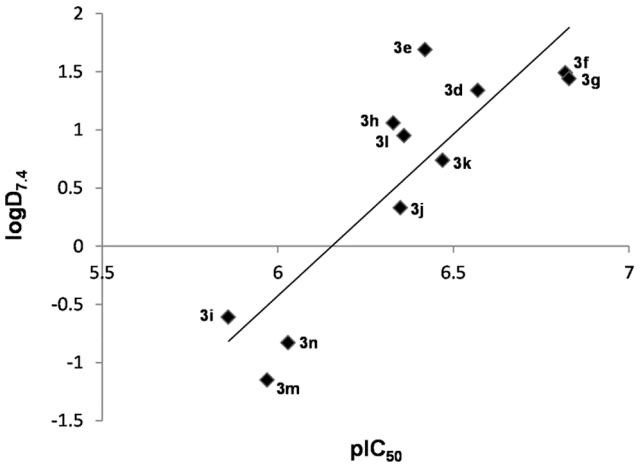

Fig. 2. $LogD_{7.4}$ values versus pIC_{50} ($-logIC_{50}$) values of DHODH inhibitory activity.

Table 4
$LogD_{7.4}$ values for **3a**-**n** obtained experimentally by shake-flask method in two-phase *n*-octanol/phosphate buffer system.

Compd.	C_1 (M)	λ (nm)	C_2 (M)	logD ± SD
3a	3.9675×10^{-5}	329	3.7866×10^{-5}	1.32 ± 0.01
3b	3.9675×10^{-5}	348	3.8030×10^{-5}	1.36 ± 0.01
3c	3.4484×10^{-5}	348	1.0314×10^{-5}	−0.37 ± 0.01
3d	3.9675×10^{-5}	350	3.7931×10^{-5}	1.34 ± 0.02
3e	2.9190×10^{-5}	356	2.8608×10^{-5}	1.69 ± 0.01
3f	2.7109×10^{-5}	348	2.6267×10^{-5}	1.49 ± 0.01
3g	2.7109×10^{-5}	348	2.6162×10^{-5}	1.44 ± 0.02
3h	2.6440×10^{-5}	348	2.4323×10^{-5}	1.06 ± 0.01
3i	3.4484×10^{-5}	348	6.7710×10^{-6}	−0.61 ± 0.01
3j	3.0014×10^{-5}	356	2.0401×10^{-5}	0.33 ± 0.02
3k	2.8187×10^{-5}	352	2.3835×10^{-5}	0.74 ± 0.01
3l	3.0355×10^{-5}	348	2.7265×10^{-5}	0.95 ± 0.01
3m	1.1377×10^{-4}	368	7.5245×10^{-6}	−1.15 ± 0.02
3n	3.3093×10^{-5}	368	4.2299×10^{-6}	−0.83 ± 0.02

C_1 - concentration of tested compound in *n*-octanol phase before partitioning (mol L^{-1});
λ - the wavelength of the absorption maximum after partitioning;
C_2 - concentration of tested compound in *n*-octanol phase after partitioning (mol L^{-1}).

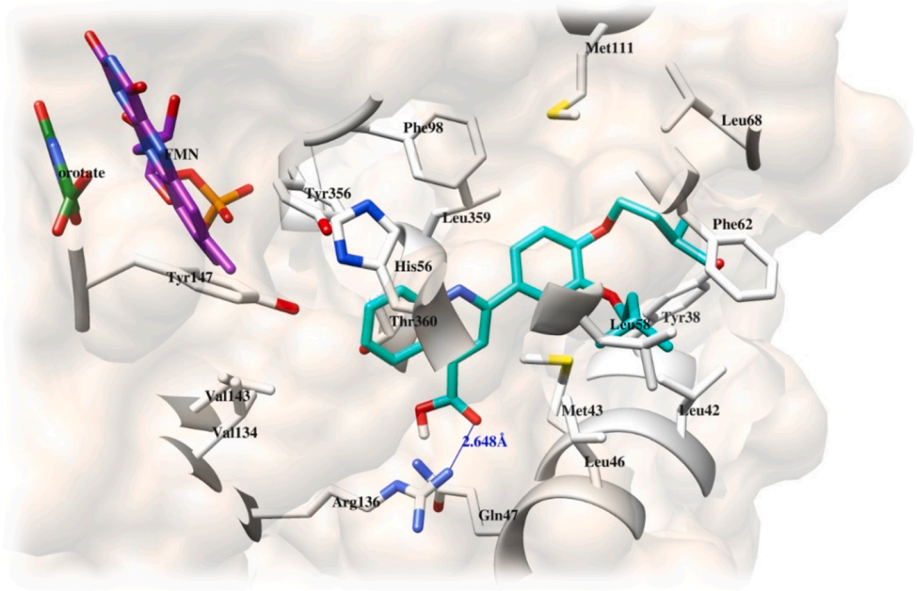

Fig. 3. The bioactive conformation of **3g** as hDHODH inhibitor. For the clarity of presentation, only the *N*-terminal amino acids, orotate as hDHODH substrate, and FMN as hDHODH coenzyme were depicted, whereas the remaining of the enzyme is illustrated with surface. Only polar hydrogens were preserved for presentation. The established hydrogen bonds are presented with blue lines. (For interpretation of the references to colour in this figure legend, the reader is referred to the web version of this article.)

most of the remaining compounds, as well, and it will be used accordingly in further discussion. The remaining hydroxyl group of the C-4 carboxylic acid scaffold is involved in electrostatic interferences with the Gln47′s amide nitrogen (another often but not an ubiquitous interaction). Consequently, the quinoline ring is placed orthogonally related to FMN and seems to seal the passage towards the coenzyme. The heterocycle's orientation is additionally conditioned with the *T*-shaped (*i.e.* edge to face) hydrophobic interactions with Val134, Val143, and Tyr356 (through the phenyl moiety), eclipsed (*i.e.* face to face) steric hindrance with Thr360′ side chain methyl group, and parallel-displaced hydrophobic interactions with His56. The quinoline's nitrogen attracts the Thr98′s side chain methyl group by means of the induced dipole of low intensity. The later described positioning of the main core is preserved with some minor alterations within the bioactive conformations of all the remaining quinoline-4-carboxylic acids. Furthermore, the extension of the quinoline in the form of another aromatic scaffold has a significant impact on the activity of **3g**. Thus, the second aromatic portion is involved, on the quinoline's nitrogen side, in the eclipsed hydrophobic interactions with Leu359 and the parallel-displaced hydrophobic interactions with Phe98, while on the C-4 carboxylic acid side the scaffold makes the repulsive interactions with Leu46 (edge to face) and Met34 (face to face). Throughout the entire set of compounds, the second aromatic scaffold more-less retains its spatial arrangement. Such constellation of the second aromatic moiety influences the C-3′ isobutyl positioning in the proximity of Leu58 and Phe62, while the C-4′ isobutyl portion is narrow to Phe62 and Leu68. The ether oxygen linkers are in both scenarios attracted by means of the electrostatic interactions with Tyr38. The bio-conformation of **3f** (Fig. 4) matches the one of **3g**. While retaining the already described hydrogen bond with ω-*N* (this time slightly weaker, d_{HB} = 2.779 Å), **3f** is narrow to the second medium strength hydrogen bond with Arg136′s δ-*N* (d_{HB} = 3.176 Å). Despite the additional advantageous interaction, the slightly lower activity of **3f** related to **3g** can be attributed to the double *n*-butyl substitution of the second aromatic moiety (*i.e.* to the absence of one methyl portion in each of the C-3′ and C-4′ substituents).

Despite embracing the comparable conformation to the ones of **3g**

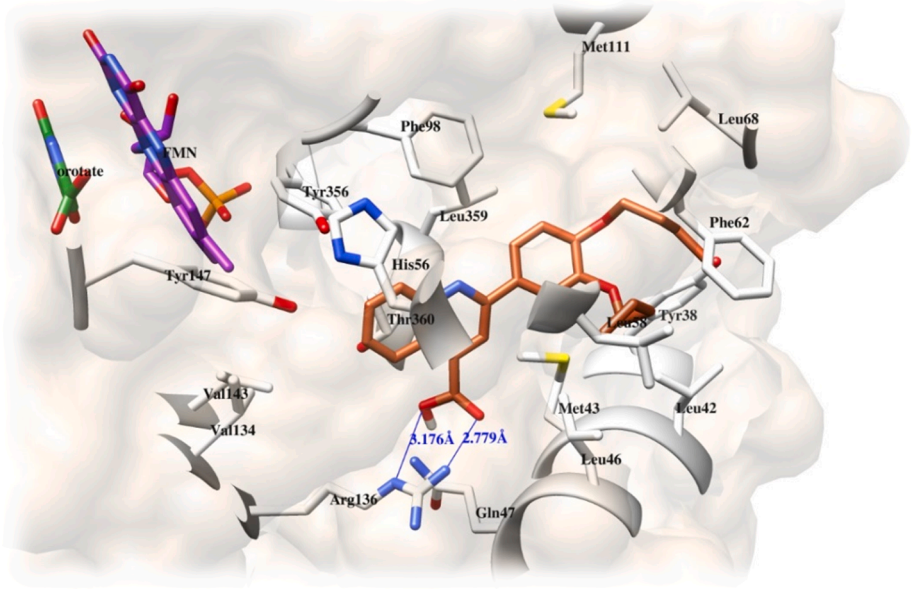

Fig. 4. The bioactive conformation of **3f** as hDHODH inhibitor. For the clarity of presentation, only the *N*-terminal amino acids, orotate as hDHODH substrate, and FMN as hDHODH coenzyme were depicted, whereas the remaining of the enzyme is illustrated with surface. Only polar hydrogens were preserved for presentation. The established hydrogen bonds are presented with blue lines. (For interpretation of the references to colour in this figure legend, the reader is referred to the web version of this article.)

and **3f**, **3a**'s lower biopotential is primary a consequence of weaker hydrogen bonds with Arg136′s ω-*N* and δ-*N* (d_{HB} = 3.279 and 3.263 Å, respectively, Supporting Information Fig. S29). Moreover, **3a**'s 2′,3′-benzyloxy disubstitution, *i.e.* the introduction of the third aromatic portion, in general, pushes the newly incorporated phenyl scaffolds towards the outskirts of the tunnel, *viz.* closer to Leu46 and Leu58 (eclipsed interactions of the 2′-substituent), Leu42 (*T*-shaped interactions of both substituents), and Phe62 (edge to face interactions of 3′-substituent). The corresponding 3′,4′-disubstitution (**3d**, Supporting Information Fig. S32) makes no significant differences within the narrow tunnel doorway, but the displacement of the C-2′-substituent to the vicinal position (*i.e.* the **3a** to **3d** transformation) causes the spatial lateral movement of the quinoline ring towards the redox site for 0.553 Å by average, ultimately causing the loss of the hydrogen bond with the Arg136′s δ-*N* and the alleviation of bioactivity in comparison with **3g** and **3f**. The importance of the proper positioning of benzyloxy scaffolds is the most expressively depicted with the consideration of **3b**'s biopose (Supporting Information Fig. S30). Thus, the benzyloxy-based 2′,4′-disubstitution for the distinct hDHODH inhibitor provides even three weak hydrogen bonds *via* the C-4 carboxylic acid in the depth of the narrow tunnel: both carbonyl and hydroxyl groups are engaged with Arg136′s ω-*N* (d_{HB} = 3.046 and 3.199 Å, respectively); hydroxyl group attracts the Arg136′s δ-*N*, as well (d_{HB} = 3.283 Å). Paradoxically, there is a decrease in the activity of **3b** related to **3d**, implying that benzyloxy substituents are perhaps too bulky for the narrow tunnel, generally speaking.

Still, the substituents of the second aromatic portion should not be spatially insignificant. Within the structure of **3k** (Supporting Information Fig. S37) there is the methoxy group at the position C-3′ and the butyloxy portion attached to the C-4′. The C-3′ portion gives low, but still a contribution while interacting with Leu46, Leu58, and Phe62, whereas the C-4′ butyloxy scaffold is more tightly bound with Phe62 and Leu68. The alleviation in bulkiness somehow increases the strength of the hydrogen bond towards the Arg136′s ω-*N* (d_{HB} = 2.647 Å), proving the later postulate. The precise hydrogen bond and the C-4′ contributors retain the activity of **3k** on a high level, although lower related to predecessors. The next ranked compound by activity is **3e** (Supporting Information Fig. S33), differing related to **3g** (Fig. 3) in the C-3′,4′-propoxy disubstitution. While the distinct substituents generate the expected hydrophobic interactions with Leu46, Leu58, Phe62, and Leu68, the **3e**'s C-4 carboxylic acid scaffold establishes even four hydrogen bonds with the sub-sites 2 and 3 (two with Arg136′s ω-*N*: d_{HB} = 2.740, and 3.206 Å, respectively; one with Arg136′s δ-*N*: d_{HB} = 3.112 Å; one with the peptide nitrogen of Thr360: d_{HB} = 2.008 Å). In other words, **3e** should be the star of the entire study. However, it seems that the reduction of C-3′,4′-disubstituents' voluminosity diminishes the **3e**'s potency on the structure-based level. Furthermore, the C-3′-methoxy group/C-4′-isobutyloxy portion ensemble is the structural marker of **3l** (Supporting Information Fig. S38), taking some features from **3k** (Supporting Information Fig. S37, the C-3′-methoxy group) and **3g** (Fig. 3, the C-4′-isobutyloxy portion). Albeit the **3l**'s hydrophobic interactions resemble the ones of **3k** (Supporting Information Fig. S37) and **3g** (Fig. 3), the inhibitor's C-4 carboxylic acid has a feature to create hydrogen bonds both with Arg136′s δ-*N* (*via* the C-4 carboxylic acid's -C═O: d_{HB} = 2.779 Å) and Gln47 (*via* the C-4 carboxylic acid's –OH: d_{HB} = 3.023 Å). Despite auspicious interactions, the opinion is that the C-3′-methoxy group existence alleviates **3l**'s biopotential. An interesting conformation was adopted by **3h** (Supporting Information Fig. S34), as well. Within, the C-3′-methoxy group has been totally overpowered by the C-4′-benzyloxy moiety, which is involved in the parallel displaced interactions with Phe62, and some weaker interactions with Leu42, Leu46, Leu58, and Leu68. The C-3′-methoxy group, as a runner up, interferes only with Phe98 and Leu359. Latter interactions and only one hydrogen bond with Arg136′s ω-*N* (d_{HB} = 2.261 Å) place this inhibitor in the midst of the herein activity scale.

The next ranked compound by means of the decreased hDHODH inhibitory activity, **3n** (Supporting Information Fig. S40), likewise establishes the corresponding hydrogen bond with Gln47 (d_{HB} = 2.908 Å), *via* the C-4 carboxylic acid's –OH, alongside with the ones with Arg136′s ω-*N* and δ-*N* (d_{HB} = 3.044 and 3.239 Å, respectively). Still, compound's significantly lower activity, related to the most active hits, is most certainly a consequence of the absence of bulky groups: the C-3′-methoxy and the C-4′-hydroxy portions have no power to engage the hydrophobic residues at the entrance of the narrow tunnel in full. The same conclusion can be made for **3m** (Supporting Information Fig. S39), as well: despite the numerous already elaborated hydrogen bonds *via* the C-4 carboxylic acid with the sub-sites 2 and 3 (two with Arg136′s ω-*N*: d_{HB} = 3.054, and 3.164 Å, respectively; one with Arg136′s δ-*N*: d_{HB} = 3.235 Å; one with Glu47: d_{HB} = 2.990 Å; one with the peptide nitrogen of Thr360: d_{HB} = 2.056 Å), the total absence of hydrophobic C-3′/C-4′ disubstituents reduces the activity of the compound in great manner. Further on, the C-2′/C-4′ disubstitution with methoxy portions (**3c**, Supporting Information Fig. S31) slightly displaces molecule and influences the reduction in a C-4 carboxylic acid-enabled hydrogen bonds number: only the one with Arg136′s ω-*N* and the bond with Glu47 remain, d_{HB} = 3.111 and 3.186 Å, respectively. The prolongation of the C-4′ substituent for two methylene residues (**3j**, Supporting Information Fig. S36), accompanied with the displacement of the methoxy scaffold form C-2′ towards C-3′, influences the formation of four C-4 carboxylic acid-provided hydrogen bonds (two with Arg136′s ω-*N*: d_{HB} = 2.713 and 3.217 Å, respectively; one with Arg136′s δ-*N*: d_{HB} = 3.122; one with Glu47: d_{HB} = 3.032 Å). Still, the non-voluminous C-3′/C-4′ disubstituents are not enough to provide the high activity against hDHODH. The importance of bulky substituents at positions C-3′ and C-4′ is the most clearly seen in the bioactive conformation of **3i** (Supporting Information Fig. S35, C-3′/C-4′-dimethoxy substitution), the least active hDHODH inhibitor, capable to establish three hydrogen bonds *via* the C-4 carboxylic acid with a narrow tunnel (one with Arg136′s ω-*N*: d_{HB} = 2.818 Å; one with Arg136′s δ-*N*: d_{HB} = 3.190 Å; one with Thr360′s peptide nitrogen: d_{HB} = 2.286 Å).

3. Conclusion

In summary, a new class of 2-substituted quinoline-4-carboxylic acids containing two alkyl/aryl ether linkages was designed, synthesized and evaluated for its hDHODH inhibitory activity and antiproliferative potential against three human cancer cells and one normal cell line. Protocatechuic aldehyde and vanillin were freely available starting compounds for a three-component Doebner reaction. Quinoline derivatives **3f** and **3g** from protocatechuic aldehyde series were the most effective hDHODH inhibitors while **3k** and **3l** from vanillin precursor had high cytotoxic activity against MCF-7 and A375 cells and good selectivity index. The presence of two hydrophobic groups such as *n*-butyl and isobutyl is crucial for excellent enzyme inhibition. However, only one hydrophobic substituent (**3k**) led to good selectivity in cytotoxic action retaining potent cytotoxicity and hDHODH inhibitory activity. Generally, good hDHODH inhibitors were also good cytotoxic agents suggesting a correlation between hDHODH inhibition and tumor cell growth particularly in A375 and MCF-7 cells. In addition, the lipophilic properties of **3a-n** significantly influence on DHODH activity because this enzyme is located in the mitochondrial membrane and compound must be able to reach to mitochondria to inhibit DHODH. The optimal lipophilicity of **3f** and **3g** with their $logD_{7.4}$ = 1.49 and 1.44 respectively was responsible for an excellent DHODH inhibition. The cytotoxic activity is mainly controlled by lipophilicity only in the narrow range of $logD_{7.4}$ values from 0.95 to 1.49. The more detailed structure-activity relationship studies were performed on the structure-based level, aiming to reveal the individual contribution of compounds' functional groups while interfering with hDHODH (in particular with the narrow tunnel within the *N*-terminal domain). Upon conducting the molecular docking, a high level of correlation between ligand-based and structure-based SAR studies was achieved. Hence, while elaborating the

interactions of either quinoline's C-4 carboxylic acid with narrow tunnel's sub-sites 2 and 3, or quinoline's C-2 Ph-C2′/C3′/C4′-disubstituents with tunnel's sub-site 1, structural characteristics responsible for providing the hDHODH inhibitory activity for any of targeted compounds were determined alongside with the guidelines for further rational design of innovative hDHODH inhibitors. The obtained bioconformations of **3a-n** were in high agreement with the previously experimentally determined crystals structures of either clinical drug leflunomide or co-crystalized 4-quinoline carboxylic acid derivatives.

4. Experimental section

4.1. Chemistry

4.1.1. Physical measurements and methods

Melting points were determined on a Mel-Temp capillary melting points apparatus, model 1001, and are uncorrected. Elemental (C, H, N, S) analysis of the samples was carried out in the Center for Instrumental Analysis, Faculty of Chemistry, Belgrade. IR spectra were obtained on a Perkin Elmer Spectrum One FT-IR spectrometer with a KBr disc. ^{1}H and ^{13}C NMR spectra were recorded on a Varian Gemini 200 MHz spectrometer. UV–Vis spectra were recorded on a double beam UV–Vis spectrophotometer model Cary 300 (Agilent Technologies, Santa Clara, USA) with 1.0 cm quartz cells.

4.1.2. General procedure for synthesis quinoline-4-carboxylic acids *3a-n*

*Procedure for the synthesis of **2a-l*** [19]. To the solution of aldehyde **1a-d** (2.2 mmol) in DMF (5 mL), K_2CO_3 (1.216 g, 8.8 mmol for **1a-c**; 0.608 g, 4.4 mmol for **1d**) was added, followed by the corresponding alkyl halide (MeI, ^{n}PrBr, ^{n}BuBr, ^{i}BuBr or BnCl) (for **1a-c** 5.07 mmol; for **1d** 2.53 mmol). The resulting mixture was then refluxed for 5 h. After completion, the suspension was filtrated, the precipitate was discarded, and 25 mL of cold water was added to the filtrate. The pH of the solution was adjusted to 4 with HCl aqueous solution (2 M), upon which a precipitate was formed in the case of compounds **2a-d**, **2g**, and **2h**. The formed suspension was then stirred for 1 h at the room temperature, filtrated, washed with a small amount of cold water, and dried over $CaCl_2$. In the case of compounds **2e**, **2f**, **2i** and **2j-l**, the solution was extracted with ethyl acetate (2 × 30 mL) after acidification, and the organic portion was dried over Na_2SO_4. Afterward, the solvent was evaporated under reduced pressure, and the obtained compounds **2e**, **2f**, **2i**, and **2j-l** were dried over $CaCl_2$. The aldehydes **2f-h**, **2j-l** were purified by column chromatography (stationary phase: silica gel, eluent: chloroform), while the other compounds **2a-e** and **2i** were obtained with satisfactory purity and were used for further synthesis without purification.

*Procedure for the synthesis of **3a-n**.* A mixture of the corresponding aldehyde **1a**, **1d**, and **2a-l** (1 mmol) and freshly distilled pyruvic acid (0.132 g, 1.5 mmol) in absolute ethanol (2 mL) was refluxed for 15 min. After cooling the flask, the solution of aniline (0.093 g, 1 mmol) in absolute ethanol (1 mL) was added, and the mixture was refluxed for 3 h. Afterward, the flask was allowed to stand at 4 °C overnight, and the formed precipitate of the corresponding compounds **3a-n** was then filtered, washed with a small amount of cold ethanol and dried over $CaCl_2$. The final compounds were obtained with satisfactory purity. However, in order to obtain compounds with very high purity, compounds **3a-d**, **3f**, **3g**, **3i**, and **3j-l** can be subjected to further purification by dissolving in a small amount of chloroform with mild heating and reprecipitation with hexane, **3n** by dissolving in acetone and reprecipitation with hexane, while **3h** can be purified by recrystallization from 70% aqueous solution of EtOH.

*4.1.2.1. 2-(2,3-Bis(benzyloxy)phenyl)quinoline-4-carboxylic acid (**3a**).* Beige powder; yield: 0.11 g (24%); mp 191–192 °C; IR (KBr, cm^{-1}): 3431, 1703, 1463, 1263, 1209, 1039, 754; ^{1}H NMR (200 MHz, DMSO-d_6): 4.93 (s, 2H, CH_2), 5.27 (s, 2H, CH_2), 7.14 (s, 5H, Ar-H), 7.25 (d, 1H, J = 8.4 Hz, Ar-H), 7.31–7.47 (m, 5H, Ar-H), 7.54–7.57 (m, 2H, Ar-H), 7.69–7.76 (m, 1H, Ar-H), 7.81–7.88 (m, 1H, Ar-H), 8.13 (d, 1H, J = 8.4 Hz, Ar-H), 8.39 (s, 1H, Ar-H), 8.73 (d, 1H, J = 8.4 Hz, Ar-H), 13.89 (bs, 1H, COOH); ^{13}C NMR (50 MHz, DMSO-d_6): 70.45, 74.92, 115.55, 122.67, 123.44, 123.84, 124.53, 125.46, 127.88 (4C), 127.98 (4C), 128.24 (2C), 128.49 (2C), 129.84 (2C), 134.07, 135.88, 136.91, 146.03, 148.46, 152.09, 155.83, 167.58; Anal. Calcd. For $C_{30}H_{23}NO_4$ (461.51 g/mol): C, 78.07; H, 5.02; N, 3.04; Found: C, 77.85; H, 4.99; N, 3.05.

*4.1.2.2. 2-(2,4-Bis(benzyloxy)phenyl)quinoline-4-carboxylic acid (**3b**).* Yellow powder; yield: 0.24 g (51%); mp 231–232 °C; IR (KBr, cm^{-1}): 3432, 1702, 1604, 1507, 1187, 1002, 698; ^{1}H NMR (200 MHz, DMSO-d_6): 5.22 (s, 2H, CH_2), 5.27 (s, 2H, CH_2), 6.84 (d, 1H, J = 8.6 Hz, Ar-H), 7.00 (s, 1H, Ar-H), 7.33–7.52 (m, 10*H*, Ar-H), 7.63–7.70 (m, 1H, Ar-H), 7.76–7.84 (m, 1H, Ar-H), 7.90 (d, 1H, J = 8.6 Hz, Ar-H), 8.11 (d, 1H, J = 8.2 Hz, Ar-H), 8.55 (s, 1H, Ar-H), 8.68 (d, 1H, J = 8.2 Hz, Ar-H), 13.78 (bs, 1H, COOH); ^{13}C NMR (50 MHz, DMSO-d_6): 69.72, 70.11, 100.97, 107.30, 121.12, 123.10, 124.05, 125.37, 127.38, 127.49 (2C), 127.82, 127.88 (2C), 128.00, 128.43 (2C), 128.53 (2C), 129.62, 129.71, 132.16, 135.35, 136.64, 136.86, 148.58, 155.64, 157.40, 160.92, 167.73; Anal. Calcd. For $C_{30}H_{23}NO_4$ (461.51 g/mol): C, 78.07; H, 5.02; N, 3.04; Found: C, 77.92; H, 5.00; N, 3.05.

*4.1.2.3. 2-(2,4-Dimethoxyphenyl)quinoline-4-carboxylic acid (**3c**).* Light yellow powder; yield: 0.11 g (36%); mp 181–182 °C; IR (KBr, cm^{-1}): 3431, 1705, 1601, 1309, 1202, 1035, 821; ^{1}H NMR (200 MHz, DMSO-d_6): 3.86 (s, 3H, CH_3), 3.90 (s, 3H, CH_3), 6.73 (d, 1H, J = 8.2 Hz, Ar-H), 6.75 (s, 1H, Ar-H), 7.63–7.71 (m, 1H, Ar-H), 7.77–7.90 (m, 2H, Ar-H), 8.11 (d, 1H, J = 8.2 Hz, Ar-H), 8.39 (s, 1H, Ar-H), 8.67 (d, 1H, J = 8.2 Hz, Ar-H), 13.84 (bs, 1H, COOH); ^{13}C NMR (50 MHz, DMSO-d_6): 55.58, 56.03, 98.89, 106.17, 120.52, 123.05, 123.78, 125.38, 127.33, 129.62, 129.69, 132.09, 135.48, 148.54, 155.72, 158.51, 161.96, 167.82; Anal. Calcd. For $C_{18}H_{15}NO_4$ (309.32 g/mol): C, 69.89; H, 4.89; N, 4.53; Found: C, 69.61; H, 4.91; N, 4.52.

*4.1.2.4. 2-(3,4-Bis(benzyloxy)phenyl)quinoline-4-carboxylic acid (**3d**).* Yellow powder; yield: 0.18 g (38%); mp 174–175 °C; IR (KBr, cm^{-1}): 3432, 1713, 1599, 1267, 1141, 1023, 734; ^{1}H NMR (200 MHz, DMSO-d_6): 5.24 (s, 2H, CH_2), 5.30 (s, 2H, CH_2), 7.24 (d, 1H, J = 8.6 Hz, Ar-H), 7.30–7.56 (m, 10*H*, Ar-H), 7.62–7.70 (m, 1H, Ar-H), 7.79–7.89 (m, 2H, Ar-H), 8.04 (s, 1H, Ar-H), 8.12 (d, 1H, J = 8.4 Hz, Ar-H), 8.41 (s, 1H, Ar-H), 8.59 (d, 1H, J = 8.4 Hz, Ar-H), 13.99 (bs, 1H, COOH); ^{13}C NMR (50 MHz, DMSO-d_6): 70.16, 70.55, 113.26, 114.32, 118.86, 120.84, 123.22, 125.44, 127.40, 127.62 (2C), 127.79 (2C), 127.90 (2C), 128.47 (4C), 129.66, 130.15, 131.10, 137.11, 137.35, 137.68, 148.36, 148.65, 150.25, 155.42, 167.79; Anal. Calcd. For $C_{30}H_{23}NO_4$ (461.51 g/mol): C, 78.07; H, 5.02; N, 3.04; Found: C, 78.13; H, 5.01; N, 3.03.

*4.1.2.5. 2-(3,4-Dipropoxyphenyl)quinoline-4-carboxylic acid (**3e**).* Yellow powder; yield: 0.11 g (30%); mp 134–135 °C; IR (KBr, cm^{-1}): 3431, 2964, 1710, 1599, 1272, 1143, 977; ^{1}H NMR (200 MHz, DMSO-d_6): 1.01 (t, 3H, J = 7.4 Hz, CH_3), 1.03 (t, 3H, J = 7.4 Hz, CH_3), 1.69–1.88 (m, 4H, $C\underline{H_2}CH_3$), 4.02 (t, 2H, J = 6.4 Hz, OCH_2), 4.08 (t, 2H, J = 6.4 Hz, OCH_2), 7.12 (d, 1H, J = 8.4 Hz, Ar-H), 7.62–7.70 (m, 1H, Ar-H), 7.78–7.90 (m, 3H, Ar-H), 8.13 (d, 1H, J = 8.2 Hz, Ar-H), 8.42 (s, 1H, Ar-H), 8.59 (d, 1H, J = 8.2 Hz, Ar-H), 13.97 (bs, 1H, COOH); ^{13}C NMR (50 MHz, DMSO-d_6): 10.54, 10.63, 22.30, 22.45, 69.94, 70.29, 112.51, 113.54, 118.80, 120.58, 123.15, 125.38, 127.28, 129.62, 130.07, 130.66, 137.54, 148.36, 148.88, 150.63, 155.54, 167.74; Anal. Calcd. For $C_{22}H_{23}NO_4$ (365.42 g/mol): C, 72.31; H, 6.34; N, 3.83; Found: C, 72.18; H, 6.36; N, 3.82.

*4.1.2.6. 2-(3,4-Dibutoxyphenyl)quinoline-4-carboxylic acid (**3f**).* Yellow powder; yield: 0.15 g (38%); mp 146–147 °C; IR (KBr, cm^{-1}): 3431,

2957, 1704, 1599, 1272, 1143, 856; ^{1}H NMR (200 MHz, DMSO-d_6): 0.95 (t, 3H, J = 7,2 Hz, CH_3), 0.96 (t, 3H, J = 7.4 Hz, CH_3), 1.38–1.59 (m, 4H, $C\underline{H_2}CH_3$), 1.67–1.82 (m, 4H, $C\underline{H_2}$ CH_2CH_3), 4.05 (t, 2H, J = 6.4 Hz, OCH_2), 4.11 (t, 2H, J = 6.4 Hz, $\underline{OCH_2}$), 7.12 (d, 1H, J = 8.6 Hz, Ar-H), 7.62–7.70 (m, 1H, Ar-H), 7.78–7.90 (m, 3H, Ar-H), 8.13 (d, 1H, J = 8.4 Hz, Ar-H), 8.42 (s, 1H, Ar-H), 8.59 (d, 1H, J = 8.4 Hz, Ar-H), 13.97 (bs, 1H, COOH); ^{13}C NMR (50 MHz, DMSO-d_6): 13.84 (2C), 18.90 (2C), 30.97, 31.10, 68.21, 68.54, 112.58, 113.58, 118.78, 120.58, 123.14, 125.36, 127.26, 129.61, 130.04, 130.68, 137.53, 148.35, 148.90, 150.67, 155.54, 167.71; Anal. Calcd. For $C_{24}H_{27}NO_4$ (393.48 g/mol): C, 73.26; H, 6.92; N, 3.56; Found: C, 72.99; H, 6.94; N, 3.55.

*4.1.2.7. 2-(3,4-Diisobutoxyphenyl)quinoline-4-carboxylic acid (**3g**).* Yellow powder; yield: 0.17 g (42%); mp 160–161 °C; IR (KBr, cm^{-1}): 3439, 2958, 1716, 1598, 1272, 1025, 801; ^{1}H NMR (200 MHz, DMSO-d_6): 1.02 (d, 6H, J = 6.6 Hz, CH_3), 1,04 (d, 6H, J = 6.6 Hz, CH_3), 1.97–2.18 (m, 2H, $C\underline{H}CH_3$), 3.83 (d, 2H, J = 6.4 Hz, OCH_2), 3.90 (d, 2H, J = 6.4 Hz, OCH_2), 7.11 (d, 1H, J = 8.4 Hz, Ar-H), 7.62–7.70 (m, 1H, Ar-H), 7.78–7.88 (m, 3H, Ar-H), 8.13 (d, 1H, J = 8.2 Hz, Ar-H), 8.42 (s, 1H, Ar-H), 8.59 (d, 1H, J = 8.2 Hz, Ar-H), 13.97 (bs, 1H, COOH); ^{13}C NMR (50 MHz, DMSO-d_6): 19.14 (2C), 19.22 (2C), 28.09, 28.25, 74.63, 75.00, 112.44, 113.50, 118.78, 120.58, 123.15, 125.38, 127.28, 129.62, 130.08, 130.67, 137.60, 148.36, 149.05, 150.78, 155.56, 167.74; Anal. Calcd. For $C_{24}H_{27}NO_4$ (393.48 g/mol): C, 73.26; H, 6.92; N, 3.56; Found: C, 73.53; H, 6.94; N, 3.57.

*4.1.2.8. 2-(4-(Benzyloxy)-3-methoxyphenyl)quinoline-4-carboxylic acid × H_2O (**3h**).* Yellow powder; yield: 0.10 g (25%); mp 182–183 °C; IR (KBr, cm^{-1}): 3438, 1708, 1600, 1373, 1272, 1024, 741; ^{1}H NMR (200 MHz, DMSO-d_6): 3.93 (s, 3H, CH_3), 5.20 (s, 2H, CH_2), 7.22 (d, 1H, J = 8.4 Hz, Ar-H), 7.32–7.52 (m, 5H, Ar-H), 7.62–7.70 (m, 1H, Ar-H), 7.79–7.93 (m, 3H, Ar-H), 8.14 (d, 1H, J = 8.4 Hz, Ar-H), 8.44 (s, 1H, Ar-H), 8.59 (d, 1H, J = 8.4 Hz, Ar-H), 13.98 (bs, 1H, COOH); ^{13}C NMR (50 MHz, DMSO-d_6): 55.90, 70.09, 110.72, 113.58, 118.83, 120.30, 123.19, 125.41, 127.33, 127.89 (2C), 127.95, 128.48 (2C), 129.64, 130.10, 131.01, 136.94, 137.65, 148.35, 149.54, 149.78, 155.51, 167.76; Anal. Calcd. For $C_{24}H_{19}NO_4 \times H_2O$ (403.43 g/mol): C, 71.45; H, 5.25; N, 3.47; Found: C, 71.19; H, 5.23; N, 3.48.

*4.1.2.9. 2-(3,4-Dimethoxyphenyl)quinoline-4-carboxylic acid (**3i**).* Yellow powder; yield: 0.08 g (26%); mp 235–236 °C; IR (KBr, cm^{-1}): 3438, 2936, 1704, 1594, 1254, 1019, 772; ^{1}H NMR (200 MHz, DMSO-d_6): 3.85 (s, 3H, CH_3), 3.92 (s, 3H, CH_3), 7.13 (d, 1H, J = 8.4 Hz), 7.62–7.70 (m, 1H, Ar-H), 7.78–7.91 (m, 3H, Ar-H), 8.13 (d, 1H, J = 8.2 Hz, Ar-H), 8.44 (s, 1H, Ar-H), 8.59 (d, 1H, J = 8.2 Hz, Ar-H), 13.97 (bs, 1H, COOH); ^{13}C NMR (50 MHz, DMSO-d_6): 55.76, 55.79, 110.39, 111.87, 118.84, 120.39, 123.19, 125.42, 127.31, 129.64, 130.10, 130.64, 137.59, 148.37, 149.20, 150.79, 155.56, 167.78; Anal. Calcd. For $C_{18}H_{15}NO_4$ (309.32 g/mol g/mol): C, 69.89; H, 4.89; N, 4.53; Found: C, 69.71; H, 4.88; N, 4.55.

*4.1.2.10. 2-(3-Methoxy-4-propoxyphenyl)quinoline-4-carboxylic acid × H_2O (**3j**).* Yellow powder; yield: 0.16 g (44%); mp 175–176 °C; IR (KBr, cm^{-1}): 3439, 2965, 1715, 1600, 1270, 1144, 1026; ^{1}H NMR (200 MHz, DMSO-d_6): 1.00 (t, 3H, J = 7.4 Hz, CH_3), 1.69–1.87 (m, 2H, $C\underline{H_2}CH_3$), 3.92 (s, 1H, CH_3), 4.01 (t, 2H, J = 6.6 Hz, OCH_2), 7.11 (d, 1H, J = 8.4 Hz, Ar-H), 7.62–7.69 (m, 1H, Ar-H), 7.78–7.91 (m, 3H, Ar-H), 8.13 (d, 1H, J = 8.2 Hz, Ar-H), 8.43 (s, 1H, Ar-H), 8.59 (d, 1H, J = 8.2 Hz, Ar-H), 13.65 (bs, 1H, COOH); ^{13}C NMR (50 MHz, DMSO-d_6): 10.56, 22.24, 55.87, 69.86, 110.67, 112.94, 118.73, 120.40, 123.14, 125.39, 127.25, 129.60, 130.06, 130.54, 137.70, 148.33, 149.35, 150.19, 155.54, 167.75; Anal. Calcd. For $C_{20}H_{19}NO_4 \times H_2O$ (355.38 g/mol): C, 67.59; H, 5.96; N, 3.94; Found: C, 67.35; H, 5.95; N, 3.95.

*4.1.2.11. 2-(4-Butoxy-3-methoxyphenyl)quinoline-4-carboxylic acid × 1.5H_2O (**3k**).* Light orange powder; yield: 0.14 g (36%); mp 180–181 °C; IR (KBr, cm^{-1}): 3468, 2940, 1703, 1598, 1371, 1278, 1025; ^{1}H NMR (200 MHz, DMSO-d_6):): 0.94 (t, 3H, J = 7.2 Hz, CH_3), 1.36–1.55 (m, 2H, $C\underline{H_2}CH_3$), 1.67–1.80 (m, 2H, $C\underline{H_2}$ CH_2CH_3), 3.91 (s, 3H, CH_3),4.04 (t, 2H, J = 6.4 Hz, OCH_2), 7.11 (d, 1H, J = 8.4 Hz, Ar-H), 7.62–7.69 (m, 1H, Ar-H), 7.78–7.90 (m, 3H, Ar-H), 8.13 (d, 1H, J = 8.2 Hz, Ar-H), 8.43 (s, 1H, Ar-H), 8.59 (d, 1H, J = 8.2 Hz, Ar-H), 13.93 (bs, 1H, COOH); ^{13}C NMR (50 MHz, DMSO-d_6): 13.84, 18.94, 30.98, 55.88, 68.08, 110.68, 112.89, 118.84, 120.41, 123.21, 125.42, 127.28, 129.64, 130.07, 130.56, 137.55, 148.40, 149.38, 150.25, 155.57, 167.78; Anal. Calcd. For $C_{21}H_{21}NO_4 \times 1.5H_2O$ (378.43 g/mol): C, 66.65; H, 6.39; N, 3.70; Found: C, 66.84; H, 6.37; N, 3.71.

*4.1.2.12. 2-(4-Isobutoxy-3-methoxyphenyl)quinoline-4-carboxylic acid (**3l**).* Yellow powder; yield: 0.10 g (29%); mp 184–185 °C; IR (KBr, cm^{-1}): 3439, 2959, 1722, 1600, 1255, 1022, 774; ^{1}H NMR (200 MHz, DMSO-d_6): 1.00 (d, 6H, J = 7.2 Hz, CH_3), 1.96–2.16 (m, 1H, $C\underline{H}CH_3$), 3.81 (d, 2H, J = 6.6 Hz, OCH_2), 3.92 (s, 3H, CH_3), 7.10 (d, 1H, J = 8.4 Hz, Ar-H), 7.62–7.69 (m, 1H, Ar-H), 7.78–7.91 (m, 3H, Ar-H), 8.13 (d, 1H, J = 8.2 Hz, Ar-H), 8.43 (s, 1H, Ar-H), 8.60 (d, 1H, J = 8.2 Hz, Ar-H), 13.96 (bs, 1H, COOH); ^{13}C NMR (50 MHz, DMSO-d_6): 19.23 (2C), 27.96, 56.00, 74.66, 110.85, 113.04, 118.83, 120.45, 123.20, 125.42, 127.27, 129.64, 130.06, 130.58, 137.54, 148.39, 150.38, 155.55, 149.42, 167.77; Anal. Calcd. For $C_{21}H_{21}NO_4$ (351.40 g/mol): C, 71.78; H, 6.02; N, 3.99; Found: C, 71.72; H, 6.03; N, 3.98.

*4.1.2.13. 2-(3,4-Dihydroxyphenyl)quinoline-4-carboxylic acid (**3m**).* Orange powder; yield: 0.10 g (34%); mp > 250 °C; IR (KBr, cm^{-1}): 3289, 2620, 1644, 1586, 1339, 1220, 876; ^{1}H NMR (200 MHz, DMSO-d_6): 6.90 (d, 1H, J = 8.2 Hz, Ar-H), 7.57–7.67 (m, 2H, Ar-H), 7.76–7.84 (m, 2H, Ar-H), 8.07 (d, 1H, J = 8.0 Hz, Ar-H), 8.32 (s, 1H, Ar-H), 8.62 (d, 1H, J = 8.0 Hz, Ar-H), 9.30 (bs, 1H, OH), 9.43 (bs, 1H, OH); ^{13}C NMR (50 MHz, DMSO-d_6): 114.53, 116.22, 118.97, 119.28, 123.29, 125.63, 127.24, 129.56, 129.66, 130.21, 137.30, 148.10, 146.05, 148.71, 156.09, 167.95; Anal. Calcd. For $C_{16}H_{11}NO_4$ (281.26 g/mol): C, 68.32; H, 3.94; N, 4.98; Found: C, 68.17; H, 3.95; N, 4.96.

*4.1.2.14. 2-(4-Hydroxy-3-methoxyphenyl)quinoline-4-carboxylic acid × 1.5H_2O (**3n**).* Brown powder; yield: 0.11 g (35%); mp 233–234 °C; IR (KBr, cm^{-1}): 3438, 2624, 1715, 1564, 1390, 1031, 759; ^{1}H NMR (200 MHz, DMSO-d_6): 3.93 (s, 3H, CH_3), 6.95 (d, 1H, J = 8.2 Hz, Ar-H), 7.60–7.68 (m, 1H, Ar-H), 7.74–7.89 (m, 3H, Ar-H), 8.11 (d, 1H, J = 8.4 Hz, Ar-H), 8.40 (s, 1H, Ar-H), 8.58 (d, 1H, J = 8.4 Hz, Ar-H), 9.57 (s, 1H, OH), 13.71 (bs, 1H, COOH); ^{13}C NMR (50 MHz, DMSO-d_6): 55.97, 111.01, 115.90, 118.74, 120.76, 123.08, 125.41, 127.12, 129.39, 129.56, 130.05, 137.56, 148.16, 148.40, 149.01, 155.82, 167.83; Anal. Calcd. For $C_{17}H_{13}NO_4 \times 1.5H_2O$ (322.32 g/mol): C, 63.35; H, 5.00; N, 4.35; Found: C, 63.01; H, 5.01; N, 4.36.

4.1.3. Determination of lipophilicity

The log$D_{7.4}$ values were experimentally obtained by the shake-flask method. A calibration graph was plotted using five different concentrations of compound in *n*-octanol. Then, 0.5 mg (for **3a**, **3b**, **3d**) or 0.8 mg (for **3c**, **3e**, **3f**, **3g**, **3h**, **3i**, **3j**, **3k**, **3l**, **3n**) of tested compounds was dissolved in 100 μl of DMSO and diluted with *n*-octanol to 25 mL in a volumetric flask. From this solution 9.154 mL (for **3a**, **3b**, **3d**) or 3.333 mL (for **3c**, **3e**, **3f**, **3g**, **3h**, **3i**, **3j**, **3k**, **3l**, **3n**) was diluted with *n*-octanol to 10 mL. The solution for **3m** was prepared by dissolving 0.8 mg in 100 μl of DMSO and diluted with *n*-octanol to 25 mL in a volumetric flask. The absorbance of the compounds in these *n*-octanol solutions was measured by UV–Vis spectrophotometry. The biphasic system containing 4 mL of previously prepared *n*-octanol solutions and 8 mL of phosphate buffer (pH = 7.4) was shaken on a mechanical shaker for 30 min. After complete phase separation, *n*-octanol layer was dried over

anhydrous sodium sulphate and absorbance was measured. The concentration was calculated from the calibration graph and $logD_{7.4}$ value was determined using equation: $logD_{7.4} = log(y/x - y)$ where x represents concentration of compound in *n*-octanol phase before shaking and y represents concentration of compound in *n*-octanol phase after the treatment on mechanical shaker. For each compound, five independent measurements were performed.

4.2. Biology

4.2.1. hDHODH inhibition assay

Recombinant human Dihydroorotate dehydrogenase (hDHODH) (Fisher Scientific, Austria) was diluted in assay buffer (50 mM Tris, 150 mM KCl and 0.8% Triton® X-100, pH 8.0, Sigma, Austria) to a final concentration of 2.5 μg/ml. The mixture was transferred into a 96-well plate. Various amounts of compounds were added and incubated for 30 min at room temperature to allow the inhibitor to react with the protein. After pre-incubation, substrate mixture (20 mM of L-DHO, 2 mM of DuQ and 1 mM of DCIP (Fisher Scientific, Austria)) was added to activate the reaction which was monitored by measuring the absorption at 610 nm using a GloMax® Multimode Microplate Reader. Leflunomide (Fisher Scientific, Austria) was used as a positive control. Each inhibitor concentration point was tested in triplicate. Finally, IC_{50} values were determined using GraphPad Prism 6.0.

4.2.2. Cell culture and cytotoxic tests

MTT, 3-(4,5-dimethylthiazol-2-yl)-2,5-diphenyltetrazolium bromide, was purchased from Sigma-Aldrich, Austria. All cell lines except A549 (ATCC: CLL-185) were a gift from Prof. Dr. Barbara Krammer, University of Salzburg (Austria). MCF-7, A375 and HaCaT cell lines were cultured in Dulbecco's modified Eagle's medium (DMEM)–high glucose supplemented with 10% fetal bovine serum, 1% penicillin–streptomycin and 1% L-glutamine. A549 cell line was maintained in Roswell Park Memorial Institute (RPMI) 1640 medium supplemented with 10% fetal bovine serum, 1% penicillin–streptomycin and 1% L-glutamine. All media and supplements were purchased from Sigma-Aldrich, Austria. Cells were grown in a humidified atmosphere at 37 °C in 5% CO_2. For all experiments, 70–80% confluent cells were used. Cells (5000 cells/well) in complete growth medium were seeded into 96-well culture plates. The day after, the medium was changed to a serum free medium with various amounts of the compounds. After an additional incubation period of 72 h, cell viability was determined by adding 10 μl MTT solution (5 mg/ml in PBS) to the compound treated and non-treated control cells for 2 h at 37 °C in the dark. Then the medium was aspirated, cells were lysed with 100 μl DMSO (VWR, Austria) and the absorbance of the resulting product formazan in viable cells was measured at 550 nm with a GloMax® Multimode Microplate Reader. Three independent experiments (with each sample in triplicate) were performed. Cell viability was normalized to the untreated control and the IC_{50} values were determined using GraphPad Prism 6.0.

4.3. Molecular docking

The molecular docking studies were conducted by means of using the human dihydroorotate dehydrogenases co-crystalized within the Protein Data Bank (Supporting Information Table S1). The docking simulations were carried out by virtue of AutoDock Vina [32] that was selected as the best performing tool for the structure-based alignment assessment of co-crystalized hDHODH inhibitors, that has been performed by using the validated protocols [33]: *Experimental Conformation Re-Docking* (ECRD), *Randomized Conformation Re-Docking* (RCRD), *Experimental Conformation Cross-Docking* (ECCD), and *Randomized Conformation Cross-Docking* (RCCD) (Supporting Information Experimental section, *Structure-based alignment assessment* sub-section).

The complexes were loaded into UCSF Chimera v1.10.1 software [34] for Linux 64-bit architecture and visually inspected. For the experimental purposes, the inhibitors were extracted from the complex, added hydrogens, and Amber parameters were calculated by means of Antechamber using semiempirical QM method. The protein parts of the saved monomers were improved by adding hydrogen atoms using the embedded leap module of Amber 12 suite [35] upon which the correct hydrogen atoms, appropriate for pH 7.4, were assigned to each amino acid residue. Upon preparation, proteins were merged with corresponding ligands and complexes were energy minimized as follows: through the leap module were solvated with water molecules (TIP3P model, SOLVATEOCT Chimera command) in a box extending 10 Å in all directions, neutralized with either Na^+ or Cl^- ions, and refined by a single point minimization using the Sander module of Amber suite with maximum 1000 steps of the steepest-descent energy minimization and maximum 4000 steps of conjugate-gradient energy minimization, with a non-bonded cutoff of 5 Å. From minimized complexes, both ligands and proteins were extracted to be used for structure-based alignment assessment and molecular cross-docking experiments. The separated proteins were used as cross-docking targets, whereas the separated inhibitors were utilized to define the cross-docking grid spacing.

The cross-docking on all of the available hDHODH proteins crystals was performed by applying the cuboid docking grid coordinates provided from hDHODH inhibitors as follows: the xyz coordinates (in Ångströms) for the computation were Xmin/Xmax = −48.696/−17.176, Ymin/Ymax = 15.078/−31.862, Zmin/Zmax = 19.960/−14.897; the coordinates setup was performed in a manner to embrace the minimized inhibitor spanning 10 Å in all three dimensions. Upon preparing the optimal grid, the following setting was used: an energy range of 10 kcal/mol and exhaustiveness of 100 with RMS Cluster Tolerance of 0.5 Å. The outputs comprised 20 different conformations. From each set of cross-docked ligands, the bioactive conformation (*i.e.* the lowest energy conformation) of an individual compound was selected by means of clustering the binding affinity values. The clinical drug leflunomide (PDB ID **3F1Q)** [30] and co-crystalized 4-quinoline carboxylic acid derivatives, brequinar (PDB ID **1D3G)** [31], **43** and **46** (PDB IDs **6CJF** and **6CJG**, respectively) [16] were used as reference bioactive conformations.

All the herein examined compounds were modelled by applying the Chemaxon's msketch module [36] by means of molecular mechanics' optimization upon which the hydrogen atoms appropriate to pH 7.4, were assigned. Upon structures' generation, compounds were uploaded into previously Vina-based molecular docking protocol to obtain the bioactive conformations.

Declaration of Competing Interest

The authors declare that they have no known competing financial interests or personal relationships that could have appeared to influence the work reported in this paper.

Acknowledgements

This work was supported by the Serbian Ministry of Education, Science and Technological Development (Agreement No. 451-03-68/2020-14/200122).

Appendix A. Supplementary data

Supplementary data to this article can be found online at https://doi.org/10.1016/j.bioorg.2020.104373.

References

[1] J.T. Madak, A. Bankhead, C.R. Cuthbertson, H.D. Showalter, N. Neamati, Revisiting the role of dihydroorotate dehydrogenase as a therapeutic target for cancer, Pharmacol. Ther. 195 (2019) 111–131.

[2] R.A.G. Reis, F.A. Calil, P.R. Feliciano, M.P. Pinheiro, M.C. Nonato, The dihydroorotate dehydrogenases: past and present, Arch. Biochem. Biophys. 632 (2017) 175–191.

[3] D.B. Sykes, The emergence of dihydroorotate dehydrogenase (DHODH) as a therapeutic target in acute myeloid leukemia, Expert Opin. Ther. Targets 22 (2018) 893–898.

[4] A. Singh, M. Maqbool, M. Mobashir, N. Hoda, Dihydroorotate dehydrogenase: a drug for the development of antimalarials, Eur. J. Med. Chem. 125 (2017) 640–651.

[5] D. Boschi, A.C. Pippione, S. Sainas, M.L. Lolli, Dihydroorotate dehydrogenase inhibitors in anti-infective drug research, Eur. J. Med. Chem. 183 (2019) 111681.

[6] M.L. Lolli, S. Sainas, A.C. Pippione, M. Giorgis, D. Boschi, F. Dosio, Use of human dihydroorotate dehydrogenase (hDHODH) inhibitors in autoimmune diseases and new perspectives in cancer therapy, Recent Pat. Anticancer Drug Discov. 13 (2018) 86–105.

[7] M.S. Dorasamy, B. Choudhary, K. Nellore, H. Subramanya, P.F. Wong, Dihydroorotate dehydrogenase inhibitors target c-myc and arrest melanoma, myeloma and lymphoma cells at S-phase, J. Cancer 8 (2017) 3086–3098.

[8] V.K. Vyas, M. Ghate, Recent developments in the medicinal chemistry and therapeutic potential of dihydroorotate dehydrogenase (DHODH) inhibitors, Mini Rev. Med. Chem. 11 (2011) 1039–1055.

[9] H. Munier-Lehmann, P.O. Vidalain, F. Tangy, Y.L. Janin, On dihydroorotate dehydrogenases and their inhibitors and uses, J. Med. Chem. 56 (2013) 3148–3167.

[10] Y.D. Fragoso, J.B. Brooks, Leflunomide and teriflunomide: altering the metabolism of pyrimidines for the treatment of autoimmune diseases, Expert Rev. Clin. Pharmacol. 8 (2015) 315–320.

[11] D.B. Sykes, Y.S. Kfoury, F.E. Mercier, M.J. Wawer, J.M. Law, M.K. Haynes, T. A. Lewis, A. Schajnovitz, E. Jain, D. Lee, H. Meyer, K.A. Pierce, N.J. Tolliday, A. Waller, S.J. Ferrara, A.L. Eheim, D. Stoeckigt, K.L. Maxcy, J.M. Cobert, J. Bachand, B.A. Szekely, S. Mukherjee, L.A. Sklar, J.D. Kotz, C.B. Clish, R. I. Sadreyev, P.A. Clemons, A. Janzer, S.L. Schreiber, D.T. Scadden, Inhibition of dihydroorotate dehydrogenase overcomes differentiation blockade in acute myeloid leukemia, Cell 167 (2016) 171–186.

[12] S. Sainas, A.C. Pippione, E. Lupino, M. Giorgis, P. Circosta, V. Gaidano, P. Goyal, D. Bonanni, B. Rolando, A. Cignetti, A. Ducime, M. Andersson, M. Järvå, R. Friemann, M. Piccinini, C. Ramondetti, B. Buccinnà, S. Al-Karadaghi, D. Boschi, G. Saglio, M.L. Lolli, Targeting myeloid differentiation using potent 2-hydroxypyrazolo[1,5-*a*]pyridine scaffold-based human dihydroorotate dehydrogenase inhibitors, J. Med. Chem. 61 (2018) 6034–6055.

[13] M. Koundinya, J. Sudhalter, A. Courjaud, B. Lionne, G. Touyer, L. Bonnet, I. Menguy, I. Schreiber, C. Perrault, S. Vougier, B. Benhamou, B. Zhang, T. He, Q. Gao, P. Gee, D. Simard, M.P. Castaldi, R. Tomlinson, S. Reiling, M. Barrague, R. Newcombe, H. Cao, Y. Wang, F. Sun, J. Murtie, M. Munson, E. Yang, D. Harper, M. Bouaboula, J. Pollard, C. Grepin, C. Garcia-Echeverria, H. Cheng, F. Adrian, C. Winter, S. Licht, I. Cornella-Taracido, R. Arrebola, A. Morris, Dependence on the pyrimidine biosynthetic enzyme DHODH is a synthetic lethal vulnerability in mutant KRAS-driven cancers, Cell Chem. Biol. 25 (2018) 705–717.

[14] P. Das, X. Deng, L. Zhang, M.G. Roth, B.M.A. Fontoura, M.A. Phillips, J.K. De Brabander, SAR-based optimization of a 4-quinoline carboxylic acid analogue with potent antiviral activity, ACS Med. Chem. Lett. 4 (2013) 517–521.

[15] M.-G.-A. Shvekhgeimer, The Pfitzinger reaction, Chem. Heterocycl. Compd. 40 (2004) 257–294.

[16] J.T. Madak, C.R. Cuthbertson, Y. Miyata, S. Tamura, E.M. Petrunak, J.A. Stuckey, Y. Han, M. He, D. Sun, H.D. Showalter, N. Neamati, Design, synthesis, and biological evaluation of 4-quinoline carboxylic acids as inhibitors of dihydroorotate dehydrogenase, J. Med. Chem. 61 (2018) 5162–5186.

[17] O. Doebner, Ueber α-alkylcinchoninsäuren und α-alkylchinoline, Justus Liebigs Ann. Chem. 242 (1887) 265–289.

[18] L.-M. Wang, L. Hu, H.-J. Chen, Y.-Y. Sui, W. Shen, One-pot synthesis of quinoline-4-carboxylic acid derivatives in water: ytterbium perfluorooctanoate catalyzed Doebner reaction, J. Fluor. Chem. 130 (2009) 406–409.

[19] N. Milhazes, T. Cunha-Oliveira, P. Martins, J. Garrido, C. Oliveira, C. Rego, F. Borges, Synthesis and cytotoxic profile of 3,4-methylenedioxymethamphetamine ("Ecstasy") and its metabolites on undifferentiated PC12 cells: a putative structure-toxicity relationship, Chem. Res. Toxicol. 19 (2006) 1294–1304.

[20] S.-F. Chen, F.W. Perrella, D.L. Behrens, L.M. Papp, Inhibition of dihydroorotate dehydrogenase activity by brequinar sodium, Cancer Res. 52 (1992) 3521–3527.

[21] S.-F. Chen, L.M. Papp, R.J. Ardecky, G.V. Rao, D.P. Hesson, M. Forbes, D.L. Dexter, Structure-activity relationship of quinoline carboxylic acids. A new class of inhibitors of dihydroorotate dehydrogenase, Biochem. Pharmacol. 40 (1990) 709–714.

[22] Y. Pan, The dark side of fluorine, ACS Med. Chem. Lett. 10 (2019) 1016–1019.

[23] S. Flis, J. Spławiński, Inhibitory effects of 5-fluorouracil and oxaliplatin on human colorectal cancer cell survival are synergistically enhanced by sulindac sulfide, Anticancer Res. 29 (2009) 435–441.

[24] J.A. Arnott, S.L. Planey, The influence of lipophilicity in drug discovery and design, Expert Opin. Drug Discov. 7 (2012) 863–875.

[25] D.A. Smith, B.C. Jones, D.K. Walker, Design of drugs involving the concepts and theories of drug metabolism and pharmacokinetics, Med. Res. Rev. 16 (1996) 243–266.

[26] J.E. Comer, High-throughput measurement of logD and pK_a, Chapter 2, in: H. van de Waterbeemd, H. Lennernäs, P. Artursson (Eds.), Drug bioavailability: estimation of solubility, permeability, absorption and bioavailability, Wiley-VCH, Weinheim, 2003.

[27] L. Hitzel, A.P. Watt, K.L. Locker, An increased throughput method for the determination of partition coefficients, Pharm. Res. 17 (2000) 1389–1395.

[28] L. Di, E.H. Kerns, Profiling drug-like properties in discovery research, Curr. Opin. Chem. Biol. 7 (2003) 402–408.

[29] B. Jeffries, Z. Wang, J. Graton, S.D. Holland, T. Brind, R.D.R. Greenwood, J.-Y. Le Questel, J.S. Scott, E. Chiarparin, B. Linclau, Reducing the lipophilicity of perfluoroalkyl groups by CF_2−F/CF_2−Me or CF_3/CH_3 exchange, J. Med. Chem. 61 (2018) 10602–10618.

[30] M. Davies, T. Heikkilä, G.A. McConkey, C.W.G. Fishwick, M.R. Parsons, A. P. Johnson, Structure-based design, synthesis, and characterization of inhibitors of human and plasmodium falciparum dihydroorotate dehydrogenases, J. Med. Chem. 52 (2009) 2683–2693.

[31] S. Liu, E.A. Neidhardt, T.H. Grossman, T. Ocain, J. Clardy, Structures of human dihydroorotate dehydrogenase in complex with antiproliferative agents, Structure 8 (2000) 25–33.

[32] O. Trott, A.J. Olson, AutoDock Vina: Improving the speed and accuracy of docking with a new scoring function, efficient optimization and multithreading, J. Comput. Chem. 31 (2010) 455–461.

[33] M. Mladenović, A. Patsilinakos, A. Pirolli, M. Sabatino, R. Ragno, Understanding the molecular determinant of reversible human monoamine oxidase B inhibitors containing 2*H*-chromen-2-one core: structure-based and ligand-based derived three-dimensional quantitative structure-activity relationships predictive models, J. Chem. Inf. Model. 57 (2017) 787–814.

[34] E.F. Pettersen, T.D. Goddard, C.C. Huang, G.S. Couch, D.M. Greenblatt, E.C. Meng, T.E. Ferrin, UCSF Chimera - a visualization system for exploratory research and analysis, J. Comput. Chem. 25 (2004) 1605–1612.

[35] D.A. Case, T.A. Darden, T.E. Cheatham III, C.L. Simmerling, J. Wang, R.E. Duke, R. Luo, R.C. Walker, W. Zhang, K.M. Merz, B. Roberts, S. Hayik, A. Roitberg, G. Seabra, J. Swails, A.W. Götz, I. Kolossváry, K.F. Wong, F. Paesani, J. Vanicek, R. M. Wolf, J. Liu, X. Wu, S.R. Brozell, T. Steinbrecher, H. Gohlke, Q. Cai, X. Ye, J. Wang, M.-J. Hsieh, G. Cui, D.R. Roe, D.H. Mathews, M.G. Seetin, R. Salomon-Ferrer, C. Sagui, V. Babin, T. Luchko, S. Gusarov, A. Kovalenko, P.A. Kollman, AMBER 12, University of California, San Francisco, 2012.

[36] Marvin Beans 15.4.27.0, 2015, ChemAxon. http://www.chemaxon.com (accessed January 2015).